Model-Based Polarimetric Target Decomposition With Power Redistribution for Urban Areas

Canbin Hu, Yifei Wang, Xiaokun Sun, Sinong Quan, and Deliang Xiang, *Member, IEEE*

***Abstract*—Polarimetric decomposition of oriented buildings is challenging due to their variable orientation angles and structures. Both vegetated and oriented built-up areas generate the HV component namely cross-polarized scattering, leading to an overestimation of volume scattering (OVS). It can cause misinterpretation of the scattering mechanisms between oriented built-up and vegetated areas. In this article, we use a pure volume scattering model designed for completely random scattering to describe the scattering of vegetated areas. At the same time, a new urban revised rate is proposed by considering the rotated dihedral model and introducing polarimetric asymmetry, which can distinguish different areas and reduce OVS in urban areas through power transfer strategy. Then, a new model-based polarimetric target decomposition with power redistribution for urban areas is proposed. The performance of our proposed method is verified by RADARSAT-2 C-band and UAVSAR L-band data. The results show that our method can not only better characterize the scattering of oriented buildings compared to previous methods but also maintain the scattering power of natural areas. It can alleviate the scattering misinterpretation problem between oriented built-up and natural areas.**

***Index Terms*—Cross-polarized scattering, oriented built-up areas, overestimation of volume scattering (OVS), polarimetric decomposition, power redistribution.**

I. Introduction

POLARIMETRIC synthetic aperture radar (PolSAR) obtains the polarimetric scattering information of different ground targets by emission and reception of vertical and horizontal electromagnetic wave [1]. As a result, it can gain the polarimetric matrix and get much comprehensive scattering information. At present, polarimetric target decomposition is an important research field of polarimetric SAR scattering mechanism analysis. In fact, the purpose of the polarimetric decomposition method is to obtain some features of scattering types. And they can make PolSAR data used more widely, such as vegetation classification [2], soil moisture estimation [3], marine monitoring [4], building information extraction [5], ship detection [6], etc. Currently, polarimetric target decomposition methods are mainly divided into two categories: decomposition based on eigenvalues and eigenvectors [7], [8], [9], and decomposition based on physical models [10], [11], [12], [13], [14], [15], [16], [17], [18], [19], [20], [21], [22], [23], [24], [25], [26]. The latter has become one of the most mainstream methods of incoherent decomposition because they display the scattering model of different ground targets in a straightforward way.

The decomposition methods based on physical models originate from Freeman and Durden (F3D) [10]. Their method forms three basic scattering types. In the F3D, all the HV scattering is described with volume scattering, which leads to the overestimation of volume scattering (OVS). In order to resolve this issue, Yamaguchi et al. [11] designed helix scattering to describe complex man-made targets, and thus, proposed the four-component decomposition to overcome the OVS. Furthermore, Sato et al. [12] improved the four-component decomposition by considering orientation angle compensation (Y4R), which has produced a favorable effect on the description of the scattering mechanisms of artificial targets. Researchers have been keen to make the different components match the characteristics of real ground covers more closely through decomposition so that they can obtain some more accurate features and apply them to subsequent studies well. In the past 20 years, many improved methods based on the original F3D and Y4R decomposition have been developed. For example, Zhang et al. [13] presented a five-component decomposition (MCSM) to improve the characterization ability of built-up area scattering. Ainsworth et al. [14] employed the split Bregman iteration to refine the model and overcame the problem of negative power. Sato et al. [15] introduced a fine volume scattering model to distinguish different types of HV scattering. An et al. [16], [27] studied polarimetric entropy to estimate the scattering information. As a result, the cross-polarized scattering produced by vegetation and building areas can be distinguished to some extent.

The main reason for the difficulty in describing the scattering characteristics of built-up areas is that oriented buildings always cause HV scattering similar to that of vegetated areas. The current polarimetric decomposition methods generally have the problem that most HV scattering generated by built-up areas are regarded as the volume scattering. Therefore, in order to overcome the problem of OVS and to distinguish the scattering

Manuscript received 13 March 2023; revised 16 May 2023 and 15 June 2023; accepted 2 September 2023. Date of publication 11 September 2023; date of current version 29 September 2023. This work was supported in part by the National Natural Science Foundation of China under Grant 62171015, in part by the Fundamental Research Funds for the Central Universities under Grant buctrc202121 and buctrc202218. *(Corresponding author: Xiaokun Sun.)*

Canbin Hu, Yifei Wang, and Xiaokun Sun are with the College of Information Science and Technology, Beijing University of Chemical Technology, Beijing 100029, China (e-mail: canbinhu@163.com; yifei_buct@163.com; sunxk@mail.buct.edu.cn).

Sinong Quan is with the College of Electronic Science, National University of Defense Technology, Changsha 410073, China (e-mail: qsnong@hotmail.com).

Deliang Xiang is with the Beijing Advanced Innovation Center for Soft Matter Science and Engineering, Beijing University of Chemical Technology, Beijing 100029, China, and also with the Interdisciplinary Research Center for Artificial Intelligence, Beijing University of Chemical Technology, Beijing 100029, China (e-mail: xiangdeliang@gmail.com).

Digital Object Identifier 10.1109/JSTARS.2023.3314129

mechanisms between built-up and vegetated areas, several decomposition methods have been proposed for urban scattering analysis of PolSAR data. Lee et al. [28] proposed polarization fraction and polarization asymmetry (PA) to capture urban and oriented urban areas in great details. Quan et al. [8] had used PA to extract buildings areas and got a higher accuracy. Ainsworth et al. [29] greatly enhanced the scattered power of artificial targets and made them better detectable according to the ratio of circular polarization correlation coefficients. And some model-based decomposition methods usually revise the volume scattering model or divide cross-polarized scattering into other scattering components. For example, An et al. [16] modeled the unitary matrix with the maximum polarization entropy and designed a new model, which shows high volume scattering power over vegetated areas. Wang et al. [17] introduced the polarization orientation angle into the probability density function to obtain a novel volume scattering model. Quan et al. [18] proposed an OOB descriptor and modified the matrix elements to describe the scattering characteristics of oriented buildings. Ratha et al. [19] designed a vegetated index using geodesic distance to evaluate the condition of crops growth. These methods are based on improving the original scattering model to achieve distinguishability of various types of ground targets basically. Unfortunately, the oriented built-up areas are still not effectively differentiated in decomposition results.

In order to separate the scattering of artificial targets from the total cross-polarized scattering, several models have been designed in recent years. Singh et al. [20] proposed dipole-like scattering models to explain T_{13}, then formed a new six-component decomposition (6SD) method. On this basis, Singh et al. [21] further proposed a new mix dipole coherence matrix, and finally, achieved the Singh seven-component scattering decomposition (7SD) method. Xiang et al. [22] modeled rotated dihedral corner reflectors for buildings with large oriented angles so that cross scattering of the oriented building areas can be separated from the overall cross-polarized scattering component. Fan et al. [23] proposed an oblique dihedral scattering model that expanded the 6SD into seven-component polarimetric decomposition. On the basis of 7SD, Malik et al. [24] introduced two scattering components by combining the dipoles, and then, proposed a nine-component decomposition method. Wang et al. [25] designed coupling scattering models to represent various scattering structure. Quan et al. [26] designed a new RICP model and proposed a seven-component decomposition with the mathematical solution method. Lee et al. [30], [31], Wang et al. [32] had proved that the model-based analysis is easily influenced by orientation angles and the relative intensities of surface and double-bounce scattering evaluated by the model-based method are slightly biased. This is the limitation of the model-based decomposition method. But it is undeniable that the cross-polarized response due to different building structures is well described according to proposed methods.

Basically, the aforementioned model-based decomposition methods added different scattering components or improved the volume scattering model. They have been proved to be effective in separating scattering produced by artificial targets from total cross-polarized scattering. However, considering the geometric structures of oriented buildings, the corresponding backscattering depends greatly on orientation angles. In fact, buildings with large orientation angles always cause cross-polarized scattering similar to vegetated areas. And they are difficult to distinguish in the result map. In order to solve it, Gan et al. [33] designed the odd and cross scattering index and proposed a two-step algorithm to distinguish each cell based on the value of both indexes. Ling et al. [34] proposed a new approach to subtracting subaperture T_{33} images from each other, which distinguished building and vegetation areas effectively. Inspired by it, we can use a rate that has great differences between different ground features to distinguish different areas and redistribute the power.

In this article, we put forward an improved decomposition method using a power redistribution strategy for urban areas. The major contributions of the article are as follows.

1) The pure volume scattering model is used and a new two-step decomposition is formed. Therefore, the volume scattering is more consistent with the actual scattering characteristics of vegetation.
2) Eigenvalue-related parameter is introduced into the model-based decomposition. The PA obtained from the eigenvalues is combined with the power obtained by model-based decomposition and an urban revised rate is proposed. Through this rate, we judge the type of ground targets and the power redistribution in oriented building areas can be achieved. The scattering in natural areas will be maintained, thus reducing OVS.
3) Cross-polarized scattering, which is recognized as volume scattering, would be redistributed to col-polarized scattering in oriented built-up areas. As a result, the extended double-bounce scattering can be enhanced to describe urban areas.

Experimental results show that our decomposition method improves the capability for scattering interpretation and better matches the scattering characteristics of the actual ground targets.

II. Methodology

A. Polarimetric Orientation Angle

In order to obtain full polarimetric information of targets, the radar system transmits and receives horizontal and vertical electromagnetic waves and conducts coherent measurement of their scattering information to form the scattering matrix S

$$\boldsymbol{S} = \begin{bmatrix} S_{hh} & S_{hv} \\ S_{vh} & S_{vv} \end{bmatrix} \tag{1}$$

where v and h stand for the vertical and horizontal polarizations. S_{hv} indicates that waves are transmitted vertically and received horizontally. Under the single station backscattering mechanism, the matrix S is symmetric, which satisfies the reciprocity theorem. The diagonal elements of the scattering matrix S represent the col-polarized terms, and the nondiagonal elements represent the cross-polarized terms. Each S matrix can be transformed into the corresponding polarimetric coherence

matrix T through the Pauli eigenvector $\boldsymbol{k}_p$ as

$$\langle |\boldsymbol{T}| \rangle = \left\langle \boldsymbol{k}_p \boldsymbol{k}_p^{\mathrm{H}} \right\rangle = \begin{bmatrix} T_{11} & T_{12} & T_{13} \\ T_{12}^* & T_{22} & T_{23} \\ T_{13}^* & T_{23}^* & T_{33} \end{bmatrix}. \tag{2}$$

The superscript H represents the conjugate transposition. $\langle\ \rangle$ represents the set average of time or space, and $*$ represents the conjugation. The target vector, namely Pauli feature vector, can be represented as

$$\boldsymbol{k}_p = \frac{1}{\sqrt{2}} \begin{bmatrix} S_{hh} + S_{vv} \\ S_{hh} - S_{vv} \\ 2S_{hv} \end{bmatrix}. \tag{3}$$

We can calculate the eigenvalues and eigenvectors of the coherence matrix T according to the following expression:

$$\langle |\boldsymbol{T}| \rangle = \sum_{\mathrm{i}=1}^{3} \lambda_i u_i u_i^H \tag{4}$$

where $\lambda_i, i = 1, 2, 3$ represents three eigenvalues of the coherence matrix T and $u_i, i = 1, 2, 3$ are unit orthogonal eigenvectors. Then, we rotate the coherency matrix by angle θ. And the rotated coherency matrix is given as

$$[T(\theta)] = [R_3(\theta)][T][R_3(\theta)]^{-1} \tag{5}$$

where $R_3(\theta)$ is a special unitary rotation operator expressed as

$$[R_3(\theta)] = \begin{bmatrix} 1 & 0 & 0 \\ 0 & \cos 2\theta & \sin 2\theta \\ 0 & -\sin 2\theta & \cos 2\theta \end{bmatrix}. \tag{6}$$

By calculation, the term T_{33} is expressed as

$$T_{33}(\theta) = T_{33}\cos^2 2\theta - \mathrm{Re}\,(T_{23}) \sin 4\theta + T_{22}\sin^2 2\theta. \tag{7}$$

The tangent of the orientation angle can be derived from $T'_{33}(\theta) = 0$ as

$$T'_{33}(\theta) = 2\,(T_{22} - T_{33}) \sin 4\theta - 4\mathrm{Re}\,(T_{23}) \cos 4\theta \tag{8}$$

$$\tan 4\theta = \frac{2\mathrm{Re}\,(T_{23})}{T_{22} - T_{33}}. \tag{9}$$

Thus, the polarimetric orientation angle θshould be written as [12]

$$\theta = \frac{1}{4}\tan^{-1}\left(\frac{2\mathrm{Re}\{T_{23}\}}{T_{22} - T_{33}}\right). \tag{10}$$

B. Pure Volume Model

In fact, volume scattering is a purely random scattering caused by a large number of complex scatterers [16]. In some cases, volume scattering model describes the random scatterers badly, leading to volume scattering power overestimation. Here, the coherence matrix conforming to the volume scattering model that is applicable to layered randomly distributed media is adopted [16]. This model assumes that the orientation angle conforms to uniform distribution. The polarimetric coherence matrix T_V can be represented as

$$\boldsymbol{T}_V = \frac{1}{3-\rho} \begin{bmatrix} 1+\rho & 0 & 0 \\ 0 & 1-\rho & 0 \\ 0 & 0 & 1-\rho \end{bmatrix} \tag{11}$$

where ρ is the related coefficient between co-pol channels

$$\frac{1+\rho}{1-\rho} = \frac{2|S_{hh} + S_{vv}|^2}{|S_{hh} - S_{vv}|^2}. \tag{12}$$

The more typical the volume scattering, the higher the randomness such as forest canopy as well as some vegetated surfaces [16]. When $\rho = 0$, it has the same eigenvalues and eigenvectors, indicating that the three components have the same power. Namely, the randomness of target is the highest, which describes the main property of volume scattering [16]. We name it pure volume scattering model. It best characterizes the randomness of the volume scattering. And we use it here. The coherence matrix T_{vol} can be expressed as

$$\boldsymbol{T}_{\mathrm{vol}} = \frac{1}{3} \begin{bmatrix} 1 & 0 & 0 \\ 0 & 1 & 0 \\ 0 & 0 & 1 \end{bmatrix}. \tag{13}$$

C. Rotated Dihedral Model

When buildings are orthogonal to the position of radar transmitting electromagnetic wave, intense double bounce scattering will produce due to the dihedral structure created by the flat ground and the wall of the artificial targets. Therefore, this kind of scattering is usually used to depict the scattering characteristic of orthogonal buildings. The dihedral scattering matrix are as follows:

$$\boldsymbol{S} = \begin{bmatrix} 1 & 0 \\ 0 & -1 \end{bmatrix}. \tag{14}$$

However, some buildings with orientations no longer present the double-bounce scattering similar to orthogonal buildings, but generate cross-polarized scattering. This scattering is usually regarded as volume scattering in many polarimetric decomposition methods. However, the cross-polarized component caused by oriented buildings is really different from that of vegetated areas. As a result, some cross-polarized scattering models designed for forests are not applicable to oriented buildings. Here, we model rotated dihedral to simulate the scattering mode of oriented buildings [12]. First, the scattering matrix S is rotated to obtain the scattering matrix

$$S(\theta) = \begin{bmatrix} \cos\theta & \sin\theta \\ -\sin\theta & \cos\theta \end{bmatrix} S \begin{bmatrix} \cos\theta & -\sin\theta \\ \sin\theta & \cos\theta \end{bmatrix}. \tag{15}$$

The rotated dihedral model assumes that the orientation angle follows the cosine distribution. Combined with the dihedral reflector, the polarimetric coherence matrix can be derived. Here, the distribution of the polarimetric angle is presented as

$$p(\theta) = \frac{1}{2}\cos(\theta - \theta_{\mathrm{dom}}), -\frac{\pi}{2} + \theta_{\mathrm{dom}} < \theta < \frac{\pi}{2} + \theta_{\mathrm{dom}} \tag{16}$$

where θ_{dom} is direction of buildings or the dominant orientation angle. The polarimetric coherence matrix of the rotated dihedral

model can be obtained as follows:

$$\langle |T| \rangle_{\text{cross}} = \begin{bmatrix} 0 & 0 & 0 \\ 0 & \frac{1}{2} - \frac{\cos(4\theta_{\text{dom}})}{30} & 0 \\ 0 & 0 & \frac{1}{2} + \frac{\cos(4\theta_{\text{dom}})}{30} \end{bmatrix}. \quad (17)$$

The cross scattering formed by the rotated dihedral model usually appears in oriented buildings, but is nonexistent in natural areas [22]. And the larger the angle is, the more the generated cross scattering is. It plays a good role in the decomposition of oriented buildings. In this article, it provides a basis for the later urban revised rate.

D. Urban Revised Rate of Oriented Buildings

Oriented buildings always produce cross-polarized scattering similar to vegetation, leading to scattering misinterpretation with vegetated areas. There are some ways to reduce the volume scattering overestimation. But there still exists much volume scattering power in oriented built-up areas. Meanwhile, the greater the angles of buildings are, the larger the volume scattering power would become. In fact, this part of existing volume scattering is unavoidable because it is related to the cross-polarized term T_{33}, making built-up areas less distinctive. When we use the urban scattering (including double-bounce scattering and scattering caused by oriented buildings) to represent the artificial targets, the built-up areas should present large scattering power. So we design an urban revised rate to redistribute the superfluous cross-polarized power to col-polarized power in urban areas and maintain the origin power in vegetated areas. By this means, the total power of col-polarized scattering would be enhanced. The original power proportion of the two components is used to decide how much power would be redistributed to surface scattering and extended double-bounce scattering, respectively. As a result, we can realize the purpose of weakening the volume scattering power in built-up areas.

For the sake of further amplifying the separability between vegetated areas and built-up areas, we introduce the polarimetric asymmetry (PA) proposed by Lee [28] as it can characterize the relative magnitude of the two polarimetric scattering mechanisms according to the ratio of sum and difference of eigenvalues. And oriented and orthogonal buildings always produce low and medium PA while natural areas have a high PA. PA is given as

$$PA = \frac{\lambda_1 - \lambda_2}{span - 3\lambda_3} \quad (18)$$

where span is the sum of all power and $\lambda_i, i = 1, 2, 3$ represents three eigenvalues of the T matrix from (4). PA is limited from 0 to 1. And we can use $(1 - \text{PA})$ to design our urban revised rate. When PA is near 0 in building areas, $(1 - \text{PA})$ is near 1. And we transfer most of volume scattering power to reduce OVS.

We try to create the urban revised rate to achieve the power compensation strategy. But the effect of just using $(1 - \text{PA})$ is not very satisfactory as it is not guaranteed that most of the values in forest area are approximately 0. The result is that large volume scattering power transfer would occur in forest area. As a result, we can add a parameter to weight $(1 - \text{PA})$, then use the power transfer strategy. Cross-polarized scattering caused by rotated dihedral model appears mainly in oriented building area and is almost absent in forest area. We add it to the urban revised rate to increase the difference between urban and forest areas and redistribute the overestimated volume scattering power. Therefore, we use the decomposed cross scattering power as a factor. And the rate r can be expressed as

$$r = (1 - PA) \cdot F(P_{\text{cro}}) \quad (19)$$

where P_{cro} is the power produced by the rotated dihedral model called cross scattering. $F(P_{\text{cro}})$ shows that r is designed as a function of P_{cro}. Since P_{cro} usually exists in urban areas and is proportional to orientation angles of buildings, the value of cross scattering power can be used as a tradeoff index for power transfer. In natural areas, cross scattering power is about 0, and r should be about 0. Under these circumstances, the cross-polarized power is not transferred basically, and scattering power in natural areas is maintained. When P_{cro} in oriented buildings is greater than 0, volume scattering power is redistributed using the ratio of r. The larger the orientation angle of buildings is, the larger the cross scattering power is. Then, the more volume scattering power caused by oriented buildings is transferred. We restrict the r as

$$r = \begin{cases} 1, r > 1 \\ 0, r < 0 \end{cases}. \quad (20)$$

In fact, most of the values of cross scattering power have a low magnitude, so the proportion of the transferred power is generally at a relatively low level. We should normalize it to a suitable extent. If cross scattering power is only used for the rate of power transfer, power transfer can only be carried out in oriented built-up areas, while other complex artificial targets still exist OVS. In order to make the decomposition method more suitable for complex geometric scattering structures, helix component proposed by Yamaguchi [11] is also introduced to the rate. The scattering component appears in inhomogeneous targets including various complex artificial structures, while it is almost absent in natural areas. Therefore, the urban revised rate r is proposed to describe urban areas

$$F(P_{\text{cro}}) = \frac{P_{\text{cro}} + P_c}{\text{mean}(\sum P_{\text{cro}} + \sum P_c) + P_{\text{cro}} + P_c} \quad (21)$$

where P_c is the helix scattering power in [11]. The $\text{mean}(\sum P_{\text{cro}} + \sum P_c)$ is the average of the total power of all cross scattering and all helix scattering for the entire area. It can be calculated as a unique value in an image and used as a tradeoff factor to weight $F(P_{\text{cro}})$ in order to keep its value at a reasonable level. When the $\text{mean}(\sum P_{\text{cro}} + \sum P_c)$ is near 0, the $F(P_{\text{cro}})$ is near 0 and it is limited from 0 to 1. The denominator is used to centralize the value of rate. Then, our urban revised rate can be expressed as

$$r = \left(1 - \frac{\lambda_1 - \lambda_2}{span - 3\lambda_3}\right) \cdot \frac{P_{\text{cro}} + P_c}{\text{mean}(\sum P_{\text{cro}} + \sum P_c) + P_{\text{cro}} + P_c}. \quad (22)$$

When high polarimetric asymmetry appears in natural areas, the first factor reaches a small amount. And the numerator of the second item is low. As a result, r is close to 0 in natural areas. In contrast, r is greater than 0 in built-up areas. And

larger orientation angles will lead to larger rate. Then, we can use the rate to decide the proportion of the transferred volume scattering power. When r tends to 1, we consider the cell as built-up area. Thus, we reduce volume scattering and increase extended double-bounce scattering to describe the scattering of urban areas. When $r = 1$, we transfer the total volume scattering power for some special areas.

Therefore, the scattering characteristics of each ground target will become distinct and the decomposition result would be clear. And it has a large power of extended double-bounce scattering in all built-up areas. As a result, volume scattering in urban areas would be weakened and it only describes the scattering mechanism of vegetated areas, thus reducing the misinterpretation between built-up areas and vegetated areas.

E. Improved Five-Component Decomposition Method

Here, the volume scattering of natural areas can be optimized using the pure volume scattering model. A rotated dihedral model is added to form a five-component decomposition. We divide the decomposition procedure into two steps. First, we use the proposed decomposition method to decompose the full-pol SAR data into five scattering components. Second, we use r to distinguish urban areas on the basis whether r is close to 1, and decide how much power to be transferred.

1) Step 1: Preliminary Formation of Five-Component Decomposition Method: We use pure volume scattering to describe the scattering from the tree canopy and add a cross-scattering component to describe oriented buildings in Step 1. A five-component decomposition method is formed as follows: the coherence matrix can be disintegrated to five components: surface scattering, double-bounce scattering, volume scattering, helix scattering, and cross scattering

$$\begin{aligned}\langle|T|\rangle &= f_s\langle|T|\rangle_{\text{surface}} + f_d\langle|T|\rangle_{\text{double}} \\ &\quad + f_v\langle|T|\rangle_{\text{vol}}^{\text{uniform}} + f_c\langle|T|\rangle_{\text{helix}} + f_{\text{cro}}\langle|T|\rangle_{\text{cross}} \\ &= f_s\begin{bmatrix}1 & \beta^* & 0\\ \beta & |\beta|^2 & 0\\ 0 & 0 & 0\end{bmatrix} + f_d\begin{bmatrix}|\alpha|^2 & \alpha & 0\\ \alpha* & 1 & 0\\ 0 & 0 & 0\end{bmatrix} \\ &\quad + \frac{f_v}{3}\begin{bmatrix}1 & 0 & 0\\ 0 & 1 & 0\\ 0 & 0 & 1\end{bmatrix} + \frac{f_c}{2}\begin{bmatrix}0 & 0 & 0\\ 0 & 1 & \pm j\\ 0 & \pm j & 1\end{bmatrix} \\ &\quad + f_{\text{cro}}\begin{bmatrix}0 & 0 & 0\\ 0 & 0.5-\frac{\cos(4\theta_{\text{dom}})}{30} & 0\\ 0 & 0 & 0.5+\frac{\cos(4\theta_{\text{dom}})}{30}\end{bmatrix} \end{aligned} \tag{23}$$

where f_s, f_d, f_v, f_c, and f_{cro} are the parameters to be solved, and five underdetermined equations containing seven unknowns can be formed by comparison on both sides. And we can get the equation as

$$\begin{aligned} \mathrm{T}_{11} &= f_s + f_d|\alpha|^2 + \frac{1}{3}f_v \\ T_{22} &= f_s|\beta|^2 + f_d + \frac{1}{3}f_v + \frac{f_c}{2} + \left(\frac{15-\cos 4\theta_d}{30}\right)f_{\text{cro}} \\ T_{33} &= \frac{1}{3}f_v + \frac{f_c}{2} + \left(\frac{15+\cos 4\theta_d}{30}\right)f_{\text{cro}} \\ \mathrm{T}_{12} &= f_s\beta^* + f_d\alpha \\ \mathrm{Im}(T_{23}) &= \frac{f_c}{2}. \end{aligned} \tag{24}$$

By referring to the solution method in [12], the dominant scattering type is judged according to the positive and negative of the real part of $S_{HH}S_{VV}^*$, so as to determine the unknown parameters. The surface scattering is considered to be dominant when the real part of $S_{HH}S_{VV}^*$ is positive, while the opposite is that double-bounce scattering is considered to be dominant. When $\mathrm{Re}(S_{HH}S_{VV}^*) > 0$

$$\begin{aligned} f_s &= |T_{12}|^2/(T_{22}-T_{33}) \\ f_v &= 3\left(T_{11} - \frac{1}{2} - |T_{12}|^2/(T_{22}-T_{33})\right) \\ f_d &= 0 \\ f_c &= 2\mathrm{Im}(T_{23}) \\ f_{cro} &= 30(T_{33} - f_v/3 - f_c/2)/(15+\cos 4\theta_d) \end{aligned} \tag{25}$$

when $\mathrm{Re}(S_{HH}S_{VV}^*) < 0$

$$\begin{aligned} f_d &= T_{22} - T_{33} \\ f_v &= 3\left(T_{11} - |T_{12}|^2/(T_{22}-T_{33})\right) \\ f_s &= 0 \\ f_c &= 2\mathrm{Im}(T_{23}) \\ f_{\text{cro}} &= 30(T_{33} - f_v/3 - f_c/2)/(15+\cos 4\theta_d). \end{aligned} \tag{26}$$

When $f_{\text{cro}} < 0$, we set cross scattering component to zero and the solution is similar to the original Sato [12]. The different scattering power can be showed as

$$\begin{aligned} P_s &= f_s(1+\beta^2), P_d = f_d(1+\alpha^2), P_v = f_v \\ P_c &= f_c, P_{\text{cro}} = f_{\text{cro}}. \end{aligned} \tag{27}$$

The preliminary five-component decomposition has added cross scattering power and we will give the result using only Step 1 in the following experimental section for comparison.

2) Step 2: Power Redistribution: Then, we use the urban revised rate to change the volume scattering power especially in built-up areas. It is meant that cross-polarized scattering caused by oriented buildings will be assigned and volume scattering caused by vegetated areas will be retained. It distributes the reduced volume scattering power to col-polarized scattering component using our method. If the rate is greater than 0, it means that there exists scattering caused by oriented buildings. And we should reduce the volume scattering here, aiming at enhancing the scattering describing oriented buildings. We use the extended double-bounce scattering to express the scattering characteristic of oriented buildings. If the reduced volume scattering is discarded directly without adding other scatterings, the principle of conservation of total scattering power will be violated. Therefore, we will determine how much the reduced

TABLE I
INFORMATION OF EXPERIMENTAL POLSAR DATA

Band of PolSAR Data	Acquisition Date	Angle of incidence
C	April 9, 2008	28°

volume scattering should be distributed to rank-1 components including surface and double-bounce scattering by the ratio of original P_d and P_s.

$$P_d^+ = P_d + \frac{P_d}{P_s + P_d} \cdot r \cdot P_v$$
$$P_s^+ = P_s + \frac{P_s}{P_s + P_d} \cdot r \cdot P_v$$
$$P_v^- = (1 - r) \cdot P_v. \tag{28}$$

We use extended double-bounce scattering to describe urban scattering, forming a new five-component decomposition method as

$$P_d^+ = P_d + \frac{P_d}{P_s + P_d} \cdot r \cdot P_v$$
$$P_s^+ = P_s + \frac{P_s}{P_s + P_d} \cdot r \cdot P_v$$
$$P_v^- = (1 - r) \cdot P_v$$
$$P_c = 2\mathrm{Im}(T_{23})$$
$$P_{cro} = 30(T_{33} - f_v/3 - f_c/2)/(15 + \cos 4\theta_d). \tag{29}$$

Through our energy transfer strategy in Step 2, the volume scattering has a different extent of decrease by the adjustment of different values of r. In forest areas, r is close to 0. The volume scattering has a less transfer. In oriented building areas, the volume scattering power is substantially transferred into rank-1 components. And the flow-process of our proposed method is shown in Fig. 1.

III. RESULTS AND DISCUSSION

In our article, the Radarsat-2 C-band data from San Francisco in California, USA and the L-band UAVSAR full polarization data in New Orleans, South Louisiana, USA are used to test our proposed method. There exist various types of features objects in the data such as oriented buildings, oceans and forests. The comparison methods adopted in this article include the latest 6SD and 7SD method proposed by Singh because they describe the scattering characteristics of buildings with different structures more comprehensively and have a better result than original Y4R.

A. Experiments on the Radarsat-2 Data

The information of the Radarsat-2 C-band data is as Table I.Fig. 2(a) displays the PolSAR Pauli image with red representing double-bounce scattering, green representing volume scattering, and blue representing surface scattering. The map of calculated polarimetric angle and optical image from Google Earth are displayed in Fig. 2(b) and (c). It is very intuitive to see

TABLE II
RESULT OF ORIENTED BUILDINGS WITH 0 ANGLES

	Patch A			
	6SD	7SD	Step 1	proposed
P_s	45.28%	44.55%	48.10%	49.98%
P_d	44.76%	41.49%	43.13%	44.62%
P_v	5.84%	10.12%	6.83%	3.46%
P_c	1.10%	0.18%	1.93%	1.93%
P_{cro}/P_{od}	1.44%	0.48%	0.01%	0.01%
P_{cd}	1.58%	0.48%	-	-
P_{md}	-	2.71%	-	-

that the oriented buildings exhibit volume-like scattering, which is similar to vegetated area.

The binary diagram of rate is presented in Fig. 2(d). Rate is rather large in built-up area. It is validated that our proposed rate can characterize the urban area and distinguish various ground targets effectively. Fig. 3(a), (b), and (d) presents the result of three methods. And Fig. 3(c) shows the preliminary decomposition result using only Step 1. Scattering types of buildings with different orientations are unified into one scattering characteristic named urban scattering. It can describe building features more accurately. In general, the proposed decomposition method out-performs the 6SD and 7SD method. From the decomposed results, we can see urban areas, those with large angles in particular, have similar scattering feature with forests as a result of OVS in 6SD and 7SD method. However, the result indicates that, by our method, it shows the similar urban scattering characteristics in most of urban areas with different orientations. They are distinguished from forest areas. And a conclusion can be drawn that the proportion of volume scattering is no longer overestimated successfully among urban areas.

In Fig. 2(d), two patches are marked with boxes of different colors to show the value of rate including urban area (blue) and natural area (yellow). The frequency histogram of the $(1 - \mathrm{PA})$ and r is shown in Fig. 4. We can see from Fig. 4(a) that (1-PA) can distinguish two areas well as their values are not exactly intersecting. It is less than 0.5 in natural area and more than 0.5 in urban area. Our proposed r has enhanced the difference between urban and natural area as shown in Fig. 4(b). It has a better effect for our decomposition. The rate is rather high in urban area, while near 0 in natural area. In this way, volume scattering would have low power transfer in forest area and large power transfer in urban area. Five areas including A-E marked with boxes representing different areas are selected to estimate the decomposed result in Fig. 3(a)–(d). Different areas represent different ground covers. A and B present the oriented buildings with 0 angles and large angles. And areas D and E show the forests and oceans, respectively.

Optical images from Google Earth corresponding to the five areas are displayed in Fig. 5. The power proportion of different scattering components using three methods and only Step 1 is presented from Tables II–VI. We can pay more attention to the contribution of various scattering to built-up area in different methods. The buildings have the same orientation with orientation angles of about 0 in patch A. When electromagnetic waves

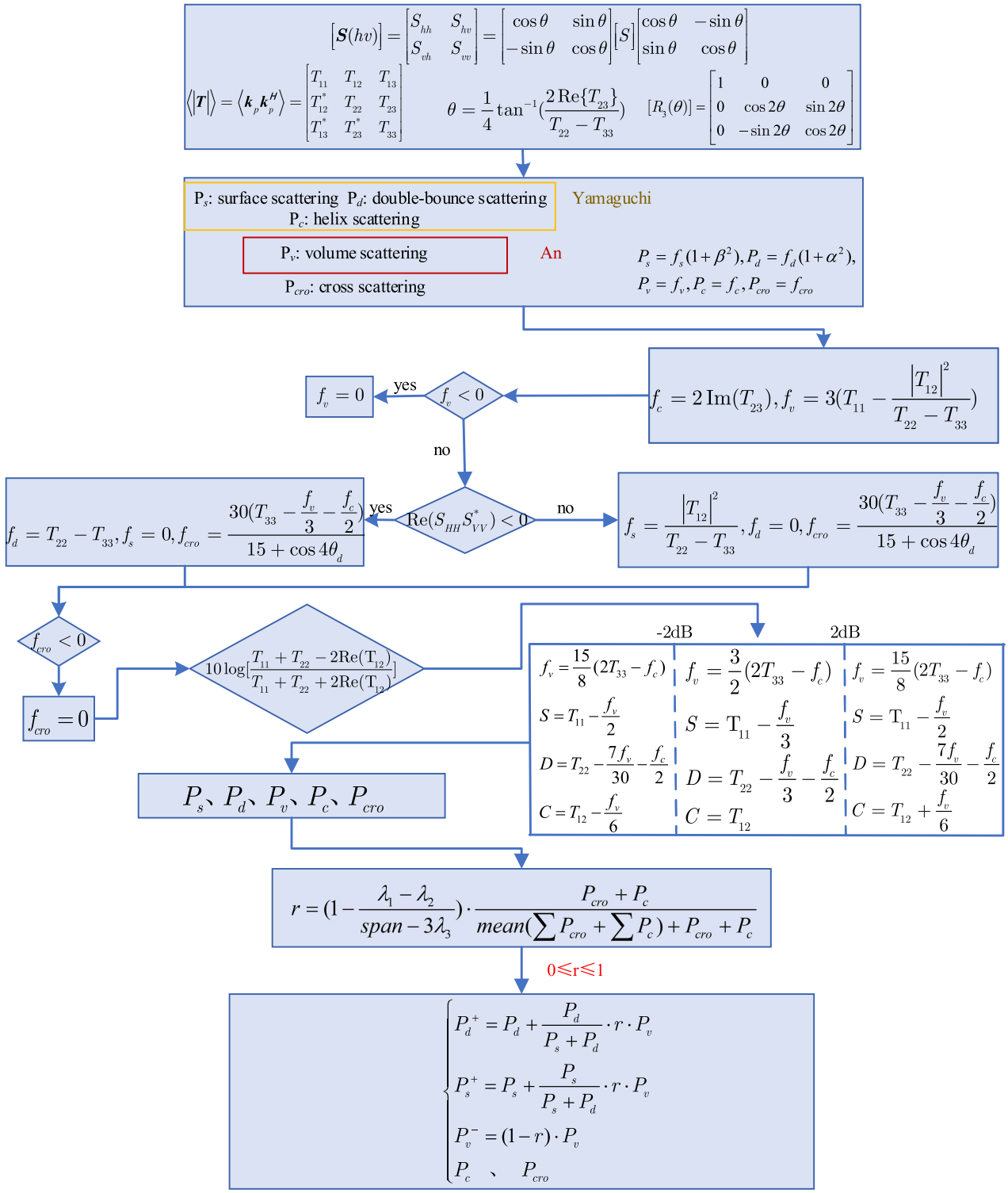

Fig. 1. Flow-process diagram of our method.

are emitted to the dihedral structure, intense double-bounce scattering will occur, which is easier to be distinguished from other scattering types. In the three methods, the surface scattering is more than 40%, which is consistent with the law that large scattering power can be generated by flat surfaces such as roofs. Meanwhile, the P_d is 44.76% in 6SD, 41.49% in 7SD, and 44.62% in the proposed method, respectively. They are similar to surface scattering power, which makes the area magenta and easy to distinguish. In 6SD and 7SD, cross scattering power is reduced by increasing the od, cd, or md scattering components, so 5.84% and 10.12% of volume scattering are obtained. In our proposed method, cross scattering power is about 0. This is because the orientation angles of buildings in area A is about 0, where there is no oriented dihedral structure. And the ratio of heilx scattering

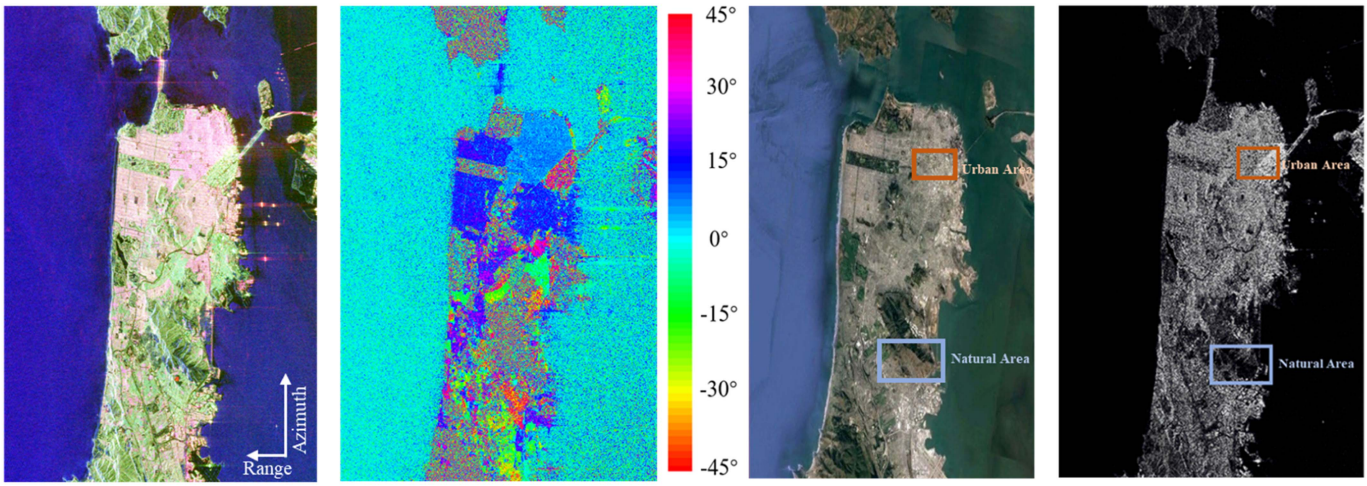

Fig. 2. PolSAR image of the study site and corresponding polarization angle map and optical image and binary diagram of rate. (a) Color-coded Pauli image with Radarsat-2 C-band data. (b) Calculated orientation angle map. (c) Optical image from Google Earth. (d) Binary diagram of rate.

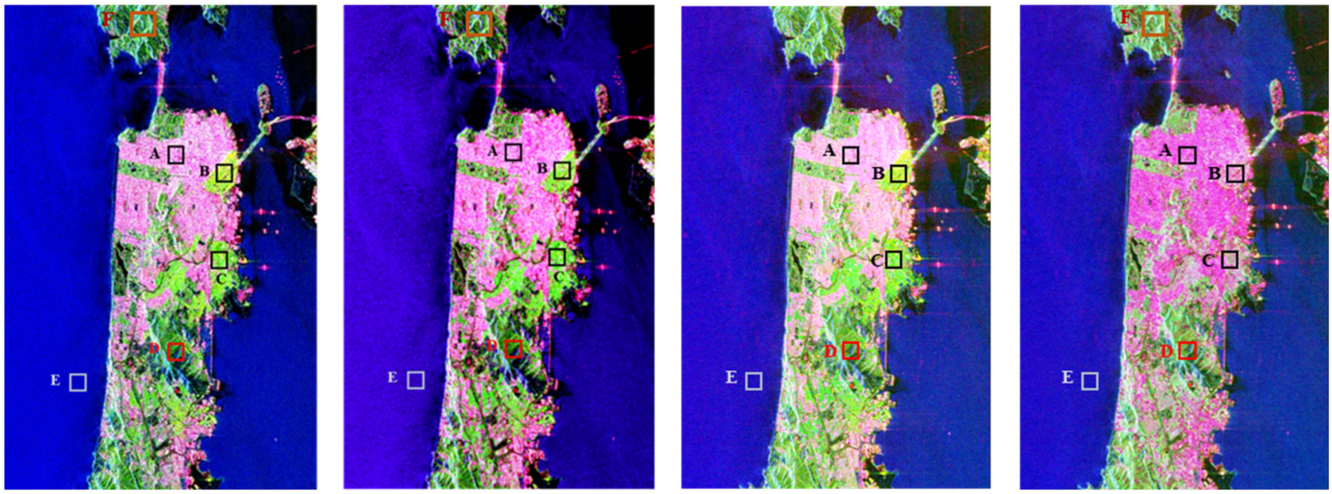

Fig. 3. Decomposition results with 6SD, 7SD, Step 1, and proposed method. (a) 6SD. (b) 7SD. (c) Result using only Step 1. (d) Proposed method. [Red: urban scattering (including double-bounce scattering, helix scattering, cross or od scattering, cd scattering, and md scattering), green: volume scattering, and blue: surface scattering.]

TABLE III
RESULT OF ORIENTED BUILDINGS WITH LARGE ANGLES

	Patch B			
	6SD	7SD	Step 1	proposed
P_s	12.46%	14.92%	12.30%	27.14%
P_d	18.81%	18.61%	12.56%	36.10%
P_v	39.11%	25.97%	52.09%	13.71%
P_c	5.01%	4.23%	5.01%	5.01%
P_{cro}/P_{od}	14.08%	11.35%	18.04%	18.04%
P_{cd}	10.53%	7.74%	-	-
P_{md}	-	17.18%	-	-

TABLE IV
RESULT OF ORIENTED BUILDINGS WITH SMALL ANGLES

	Patch C			
	6SD	7SD	Step 1	proposed
P_s	9.84%	17.59%	9.55%	50.23%
P_d	4.52%	2.18%	2.59%	20.72%
P_v	54.65%	41.80%	78.22%	19.41%
P_c	5.61%	5.21%	4.76%	4.76%
P_{cro}/P_{od}	15.51%	10.88%	4.88%	4.88%
P_{cd}	9.87%	7.87%	-	-
P_{md}	-	14.47%	-	-

power is 1.93%. And the result at the end of the Step 1 is similar to that of 6SD and 7SD in area A. Therefore, in order to enhance the scattering characteristics of orthogonal buildings, we make further efforts to reduce the volume scattering power by rate balanced mainly by helix scattering power so that the volume scattering is reduced to 3.46%. Compared with 7SD, it increases the power of col-polarized power.

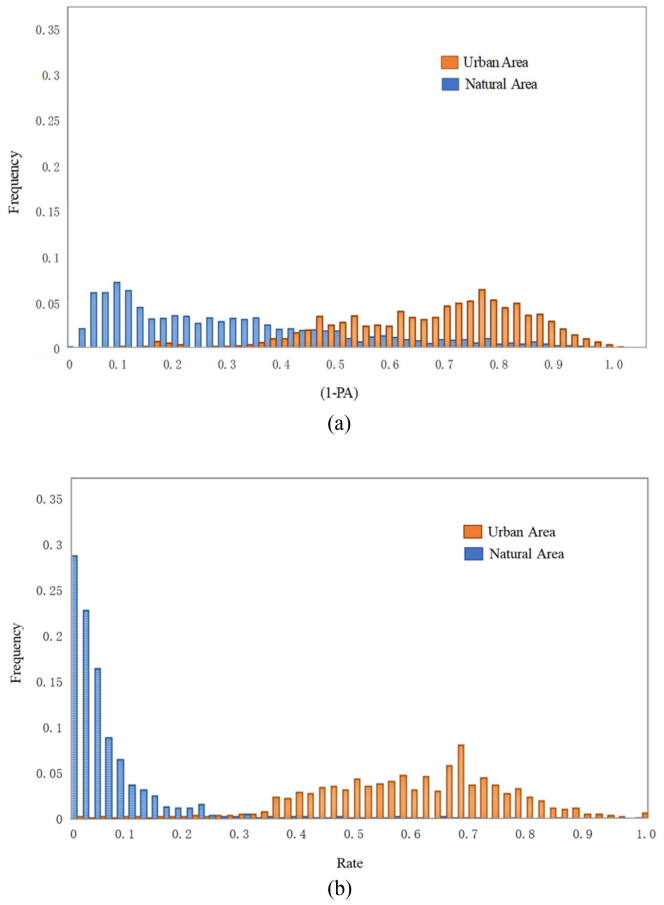

Fig. 4. Histograms of the (1-PA) and Rate in two areas. (a) (1-PA), (b) Rate.

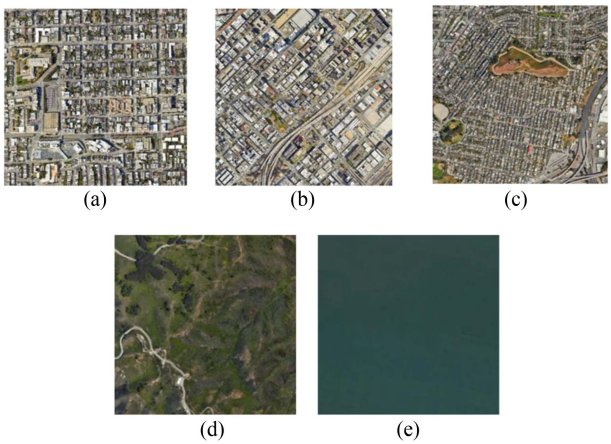

Fig. 5. Optical images from Google Earth corresponding to the selected areas. (a)–(e) Patch A–E.

Area B includes buildings with angles of about 45°. 6SD and 7SD model the dipoles of different structures by adding more than 20% od, cd, or md to describe oriented buildings as much as possible. But the oriented buildings generate more cross-polarized scattering inevitably. And it is shown that the volume scattering power accounts for 39.11% and 25.97% in 6SD and 7SD, respectively. And it is still dominant among all scattering components. As a result, volume scattering power occupies a relatively high percentage, which shows the similar characteristics with vegetated area. It causes misinterpretation between the two types of ground targets. And P_v has reached 52.09% in Step 1 and oriented built-up area shows large volume scattering power, which has caused OVS. In fact, it is unavoidable that cross-polarized scattering generated by oriented buildings is always regarded as volume scattering. In our proposed method, the cross scattering reaches 18.04% in oriented built-up area, which makes the rate reach a high value. We redistribute excess volume scattering to col-polarized scattering and reduce volume scattering power to 13.71%. Compared with 6SD and 7SD, P_s increases by over 10%, and P_d increases more than twice times. Extended double-bounce scattering dominates in area B, which shows the similar decomposed result with orthogonal buildings and improves the ability to describe oriented built-up area.

TABLE V
RESULT OF FOREST

	Patch D			
	6SD	7SD	Step 1	proposed
P_s	18.85%	23.55%	27.77%	36.25%
P_d	10.63%	7.90%	7.94%	12.86%
P_v	46.29%	41.25%	58.13%	44.73%
P_c	6.73%	5.48%	5.45%	5.45%
P_{cro}/P_{od}	8.61%	8.07%	0.71%	0.71%
P_{cd}	8.89%	7.45%	-	-
P_{md}	-	6.30%	-	-

TABLE VI
RESULT OF OCEAN

	Patch E			
	6SD	7SD	Step 1	proposed
P_s	83.65%	94.23%	94.90%	94.93%
P_d	3.27%	2.22%	2.72%	2.72%
P_v	3.39%	3.49%	1.96%	1.93%
P_c	3.23%	0.01%	0.42%	0.42%
P_{cro}/P_{od}	3.23%	0.02%	0.00%	0.00%
P_{cd}	3.23%	0.02%	-	-
P_{md}	-	0.01%	-	-

Area C includes buildings with orientation angles of about 15°. It belongs to buildings with small angles. The decomposition results of three comparison methods show high volume scattering, which is 54.65% in 6SD. This part of volume scattering has reached half, even greater than the proportion of volume scattering in forest in area D. Volume scattering is reduced to 41.8% in 7SD by increasing the md scattering component. In the two methods, P_s is 9.84%, 17.59%, and P_d is 4.52% and 2.18%, respectively. P_s is greater than P_d, because the buildings with small orientation angles make the radar echo signal more random. Therefore, some reflections from the flat areas, including the surface scattering from the roof of the building, will also generate greater power. As the orientation angle decreases, the scattering of different dipoles increases. Od scattering is more than 10% in both decomposition, which indicates that 45° dipole scattering can describe oriented buildings with small angles. The

previous decomposition method did not address the OVS for buildings with small orientation angles. And our preliminary decomposition method using only Step 1 still exhibits strong volume scattering power in the area. Through our power transfer after two steps, the decomposition result is more reasonable. The volume scattering is lower after Step 2 as we transfer volume scattering to other scattering components.The proportion of volume scattering has been reduced by more than 50% in the proposed method, which shows that it can overcome OVS in oriented buildings with small angles. The proportion of cross scattering is 4.88%, which is smaller than that of area B. It is consistent with the law of cross scattering to orientation angles. Compared with 6SD and 7SD, P_d is increased by more than five times, and the surface scattering power is also risen. P_d and P_s reach to 50.23% and 20.72%, respectively. It accords with the characteristics of built-up area better. Conclusion can be drawn from Table IV that volume scattering power of the urban area decreases due to the partial distribution on rank-1 scattering components in the proposed method and clearer docomposition result is acquired.

Area D includes forests, so volume scattering occupies a large proportion. The proportions of P_v are 44.73% in the proposed method as shown in Table V. And P_v has a similar proportion in four methods. We can see that P_v in 7SD is slightly lower than that in 6SD. This is because the joining of the mixed dipole model takes away part of the cross-polarized scattering. It can be seen from Table V that P_{cro} is low, so volume scattering power transfer would be low. P_v is 58.13% in Step 1 and still dominant. It is slightly lower after Step 2 in our proposed method. But we can still keep P_v in forest area dominant and the largest in all areas using our proposed method. As a result, volume scattering is basically maintained compared with 6SD and 7SD as shown in Table V. However, there are still the alike matter with the original Yamaguchi. Surface scattering power can reach 36.25% using our proposed method. As it has similar solution with Yamaguchi, which leads to a large portion of P_s, so we allocate more power to P_s.

Patch E includes ocean, which shows large surface scattering power in decomposition results. The proportion of surface scattering power is above 94% except 6SD in decomposition methods, which is in line with the characteristics of specular reflection of ocean water bodies. And the formation of waves is very likely to cause the generation of a small amount of double-bounce scattering rather than other scattering. Our method achieves the reduction of P_v. It has been more accurate to describe the scattering characteristics of ocean.

Overall, the double-bounce scattering is enhanced in urban area effectively by using our proposed method, yet increased surface scattering power seems not so reasonable. As building roofs lead to large surface scattering power, it is acceptable. As a result of the decreased volume scattering power, more cells can be discriminated between urban and natural area. Compared with other methods, the results show that the scattering properties of ground features can be reflected well in our proposed method. And it has a breakthrough in decomposition results as it can achieve the purpose that urban buildings have a unified scattering characteristic. And this is attributed to power transfer.

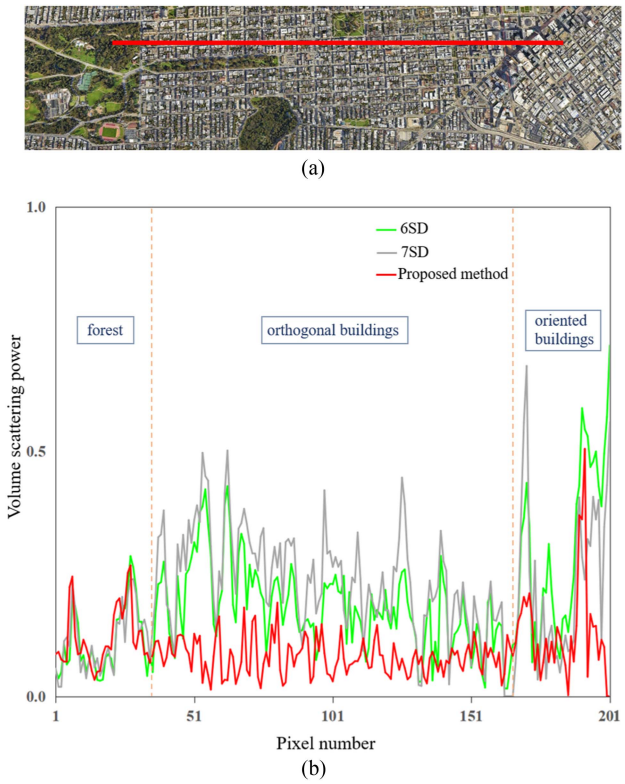

Fig. 6. (a) Image by GoogleEarth. (b) Comparison of volume scattering power in different methods.

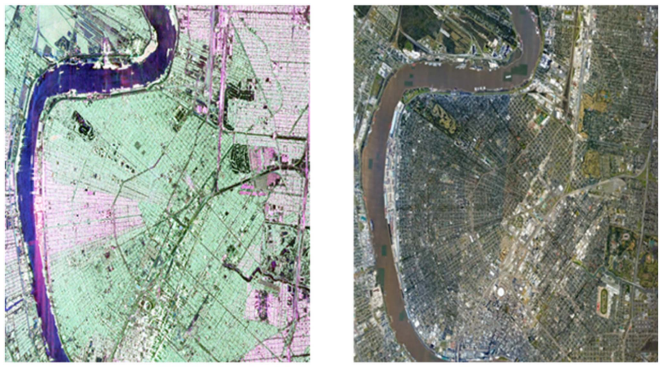

Fig. 7. PolSAR data and the optical image from GoogleEarth. (a) Pauli coded UAVSAR data. (b) Corresponding optical image from GoogleEarth.

The performance of three methods is compared by observing the volume scattering power of forest, orthogonal buildings, and oriented buildings in Fig. 6. We mark the measured area with a red strip in Fig. 6. Conclusion can be drawn that volume scattering in vegetated area is similarly large, but quite different in two different urban areas. It is rather high in 6SD and 7SD, even higher than forest. In fact, it should not show large volume scattering in built-up area. As a result, P_v is reduced to a large extent using the proposed method, and part of them is distributed to surface and double-bounce scattering power by our proposed urban revised rate.

In order to verify that the proposed method of this article can effectively maintain volume scattering power of vegetation

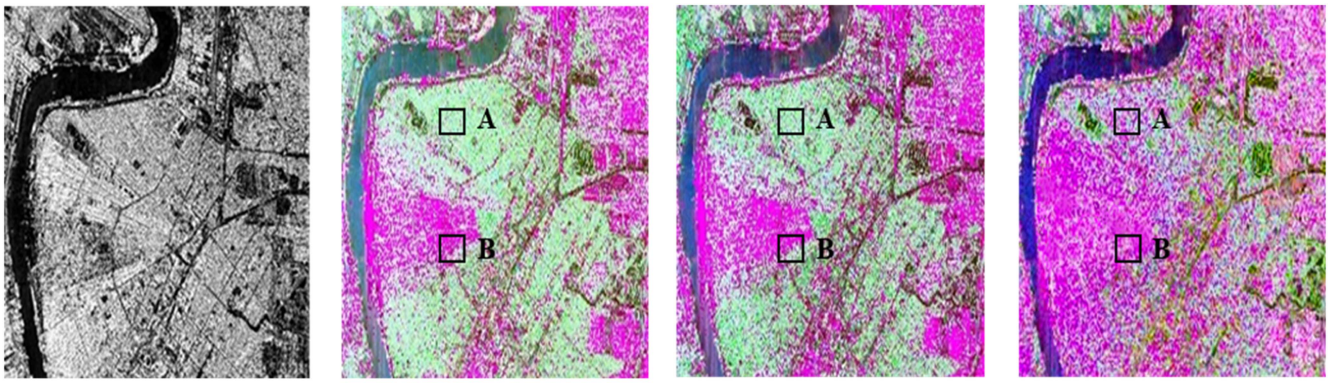

Fig. 8. Rate binary diagram and decomposition results with different methods for PolSAR data over New Orleans, LA, USA. (a) Rate of the proposed method. (b) 6SD. (c) 7SD. (d) Proposed method.

TABLE VII
RESULT OF VEGETATION AREA

	Patch F		
	6SD	7SD	proposed
P_s	23.33%	26.64%	33.95%
P_d	10.84%	8.63%	14.85%
P_v	46.23%	42.43%	45.91%
P_c	4.45%	3.66%	4.29%
P_{cro}/P_{od}	8.05%	6.90%	1.00%
P_{cd}	7.10%	7.08%	-
P_{md}	-	4.67%	-

area while solving the problem of OVS in oriented built-up area, the quantitative analysis of another forest area based on Radarsat-2 C-band data is carried out in this section. We marked patch F in Fig. 3(a), (b), and (d). The proportional statistics of each component have been shown in Table VII. It can be found that among the three methods, the proportion of volume scattering in our proposed method can be maintained basically, which indicates that this method can adequately extract the dominant scattering components of the forest area. Thus, the decomposition results are consistent with the actual scattering process according to our method.

B. Experiments on the UAVSAR Data

To further valid the availability of our method, the L-band UAVSAR full polarization data are used here. The size of data is 3300×19051 pixels. It was obtained in May 2015 with an azimuthal resolution of 7.3 m and a distance resolution of 6.7 m. The study site is located in New Orleans, LA, USA, which contains dense urban areas with different orientation angles and natural areas. Due to the large image size, this article first selects the part of the data (1127×1181 pixels). It contains urban buildings with different orientation angles from Fig. 7 and is used to verify the effect of our method in this article on the OVS of urban areas.

Fig. 7(a) is Pauli color-coded image. Fig. 7(b) is the actual figure map of the area. From the two images, we can observe that the area contains various buildings with different orientation angles.

The rate binary diagram and three decomposed results are displayed in Fig. 8, where red represents urban scattering. Two black boxes are marked out. And in Table VIII, the mean power of different methods is shown. Fig. 8(a) shows the value map of rate.

It is observed from Fig. 8, area A includes buildings with large angles. We can see that surface scattering dominates among three decomposition methods. It has a proportion of 30.73% in 6SD. However, volume scattering can reach large power comparable to surface scattering. It indicates that there is a serious problem of OVS in oriented built-up area in 6SD. The 7SD method separates the cross scattering by designing md, which reduces volume scattering by about 2%. However, volume scattering power is still large in the decomposition results. It is observed from Fig. 8(d), with the improvement of our method by power redistribution, oriented buildings show more extended double-bounce scattering in urban area. Table VIII shows that patch A has relatively low cross scattering, so we use our balanced rate to complement the power transferred. P_v is decreased to 15.15%, which shows that our method is effective in improving OVS in oriented built-up area. A part of volume scattering is transferred to col-polarized scattering. Therefore, P_s and P_d are increased by about 10% compared to 6SD and 7SD.

Patch B includes buildings with small orientation angle about 15° in Fig. 8. From Fig. 8(b)–(d), conclusion can be drawn that area B shows large urban scattering in all three methods. It indicates that buildings with small angles generate less volume scattering. Meanwhile, P_v does not account for a high proportion in patch B in Table VIII. Volume scattering accounts for 15.01% in 6SD, which is less than P_s and P_d. And P_d accounts for a large proportion in 6SD, while P_v increases and surface scattering dominates in 7SD. In fact, both of P_s and P_d are high in patch B with similar percentages. It is because buildings with small orientation angles make the radar echo signal more random. The dihedral structures still generate double-bounce scattering. And it has some wide roads between buildings in this area, which makes the surface scattering higher. With the improvement of the proposed method, we reduce volume scattering to 6.12% and

TABLE VIII
RESULT OF ORIENTED BUILT-UP AREAS WITH LARGE ORIENTATION ANGLES (A) AND SMALL ORIENTATION ANGLES (B)

	Patch A			Patch B		
	6SD	7SD	proposed	6SD	7SD	proposed
P_s	30.73%	31.97%	48.13%	35.83%	34.99%	44.55%
P_d	22.46%	21.32%	32.20%	38.57%	33.98%	42.62%
P_v	30.50%	28.66%	15.15%	15.01%	21.07%	6.12%
P_c	3.87%	3.44%	4.45%	4.47%	3.00%	6.71%
P_{cro}/P_{od}	6.68%	5.76%	0.08%	2.52%	1.28%	0.01%
P_{cd}	5.77%	5.47%	-	3.60%	1.97%	-
P_{md}	-	3.38%	-	-	3.70%	-

(a) (b) (c)

Fig. 9. Decomposed results with different methods for PolSAR data over New Orleans, LA, USA. (a) 6SD. (b) 7SD. (c) Proposed method.

(a) (b)

Fig. 10. Corresponding optical image. (a) Oriented bridge. (b) Oriented ships.

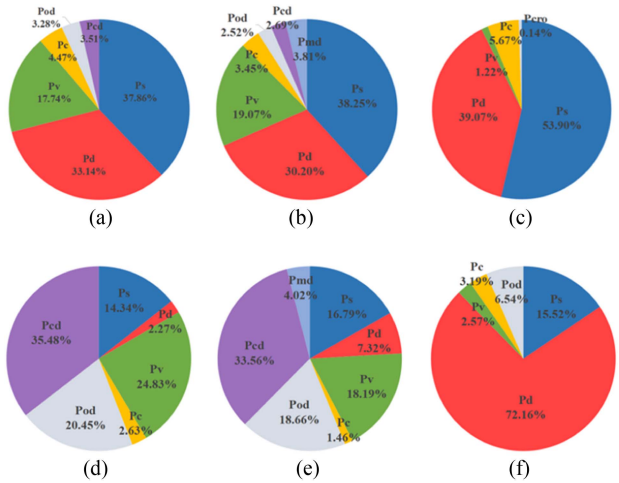

Fig. 11. Percentage of mean power for three decomposition results in 6SDand 7SD in the selected patches. (a)–(c) 6SD, 7SD, and proposed method for the oriented bridge. (d)–(f) 6SD, 7SD, and proposed method for oriented ships.

improve the power of col-polarized components by about 10%, the proposed method makes the decomposition results more correspond to the real scattering characteristics of the area.

Overall, comparing to the previous decomposition methods, our method performs better in overcoming OVS in urban area. It is because we focus more on transferring volume scattering power caused by buildings to col-polarized scattering components directly in urban area depending on the urban revised rate. Our proposed method has the advantage of greatly reducing volume scattering, so well as enhancing surface scattering and extended double-bounce scattering in built-up area. As a result, it can show large urban scattering in built-up area and maintain the scattering power of natural area.

We add some experiments containing different artificial target area in Fig. 9, where red shows urban scattering. In fact, the proposed method is not only applicable to oriented buildings but also has better results for all oriented artificial targets. It is due to the fact that artificial targets with large orientations always produce cross-polarized scattering, which is regarded as volume scattering, making the decomposition easily misinterpreted like Fig. 9(a) and (b). We have selected oriented bridge and oriented ships and marked them with yellow boxes in Fig. 9. And Fig. 10 shows the selected areas. In 6SD and 7SD, since both targets have large orientation angles, they do not show a better result in 6SD and 7SD. Especially ships show large volume scattering power. By our new method of energy transfer, we reduce volume scattering of oriented bridge and oriented ships so that they show more urban scattering in the decomposition. The result of mean power statistics using three methods are displayed in Fig. 11 to authenticate our proposed method.

IV. CONCLUSION

In this article, a new polarimetric decomposition method applying for urban areas with power redistribution is proposed based on fully polarimetric SAR data. We introduce rotated dihedral model to derive corresponding coherence matrix. Then, we design an urban revised rate by PA and parameter by model-based decomposition to balance the power, which is transferred and received in urban area. It can describe buildings with different orientation angles and differentiate built-up areas and other areas effectively. We can intuitively see that volume scattering power is transferred while surface and extended double-bounce scattering power are grown in urban areas. Our improved method with power redistribution is effective in reducing OVS of built-up

areas. Meanwhile, the scattering components of natural areas are unaffected basically.

In summary, the proposed decomposition method can decrease the ambiguity of the scattering mechanisms and better match the scattering characteristics of different ground targets. Therefore, it can better distinguish built-up and natural areas in our decomposition result.

REFERENCES

[1] R. Yang, B. Dai, and H. Li, "Polarization hierarchy and system operating architecture for polarimetric synthetic aperture radar," *J. Radars*, vol. 5, no. 2, 2016, Art. no. 132.

[2] Q. Yin, W. Hong, F. Zhang, and E. Pottier, "Optimal combination of polarimetric features for vegetation classification in PolSAR image," *IEEE J. Sel. Topics Appl. Earth Observ. Remote Sens.*, vol. 12, no. 10, pp. 3919–3931, Oct. 2019, doi: 10.1109/JSTARS.2019.2940973.

[3] H. Shi et al., " Soil moisture retrieval over agricultural fields from L-band multi-incidence and multitemporal PolSAR observations using polarimetric decomposition techniques," *Remote Sens. Environ.*, vol. 261, 2021, Art. no. 112485.

[4] J. Fan, J. Zhao, W. An, and Y. Hu, "Marine floating raft aquaculture detection of GF-3 PolSAR images based on collective multikernel fuzzy clustering," *IEEE J. Sel. Topics Appl. Earth Observ. Remote Sens.*, vol. 12, no. 8, pp. 2741–2754, Aug. 2019, doi: 10.1109/JSTARS.2019.2910786.

[5] D. Pirrone, S. De, A. Bhattacharya, L. Bruzzone, and F. Bovolo, "An unsupervised approach to change detection in built-up areas by multitemporal PolSAR images," *IEEE Geosci. Remote Sens. Lett.*, vol. 17, no. 11, pp. 1914–1918, Nov. 2020, doi: 10.1109/LGRS.2019.2958262.

[6] T. Zhang, S. Quan, W. Wang, W. Guo, Z. Zhang, and W. Yu, "Information reconstruction-based polarimetric covariance matrix for PolSAR ship detection," *IEEE Trans. Geosci. Remote Sens.*, vol. 61, Feb. 2023, Art no. 5202815, doi: 10.1109/TGRS.2023.3242078.

[7] C. Wang, W. Yu, R. Wang, Y. Deng, and F. Zhao, "Comparison of nonnegative eigenvalue decompositions with and without reflection symmetry assumptions," *IEEE Trans. Geosci. Remote Sens.*, vol. 52, no. 4, pp. 2278–2287, Apr. 2014, doi: 10.1109/TGRS.2013.2259177.

[8] S. Quan, B. Xiong, D. Xiang, L. Zhao, S. Zhang, and G. Kuang, "Eigenvalue-based urban area extraction using polarimetric SAR data," *IEEE J. Sel. Topics Appl. Earth Observ. Remote Sens.*, vol. 11, no. 2, pp. 458–471, Feb. 2018, doi: 10.1109/JSTARS.2017.2787591.

[9] F. Zhu, Y. Zhang, and D. Li, "Eigenvalue/eigenvector-based serial decomposition of the polarimetric synthetic aperture radar coherency matrix," *IET Radar Sonar Navigation*, vol. 12, no. 2, pp. 209–217, 2018.

[10] A. Freeman and S. L. Durden, "A three-component scattering model for polarimetric SAR data," *IEEE Trans. Geosci. Remote Sens.*, vol. 36, no. 3, pp. 963–973, May 1998, doi: 10.1109/36.673687.

[11] Y. Yamaguchi, T. Moriyama, M. Ishido, and H. Yamada, "Four-component scattering model for polarimetric SAR image decomposition," *IEEE Trans. Geosci. Remote Sens.*, vol. 43, no. 8, pp. 1699–1706, Aug. 2005.

[12] A. Sato, Y. Yamaguchi, G. Singh, and S. E. Park, "Four-component scattering power decomposition with extended volume scattering model," *IEEE Geosci. Remote Sens. Lett.*, vol. 9, no. 2, pp. 166–170, Mar. 2012.

[13] L. Zhang, B. Zou, H. Cai, and Y. Zhang, "Multiple-component scattering model for polarimetric SAR image decomposition," *IEEE Geosci. Remote Sens. Lett.*, vol. 5, no. 4, pp. 603–607, Oct. 2008.

[14] T. L. Ainsworth, Y. Wang, and J. S. Lee, "Model-based polarimetric SAR decomposition: An L1 regularization approach," *IEEE Trans. Geosci. Remote Sens.*, vol. 60, Jun. 2021, Art. no. 5208013, doi: 10.1109/TGRS.2021.3083511.

[15] A. Sato, Y. Yamaguchi, G. Singh, and S. E. Park, "Four-component scattering power decomposition with extended volume scattering model," *IEEE Geosci. Remote Sens. Lett.*, vol. 9, no. 2, pp. 166–170, Mar. 2012.

[16] W. An, Y. Cui, and J. Yang, "Three-component model-based decomposition for polarimetric SAR data," *IEEE Trans. Geosci. Remote Sens.*, vol. 48, no. 6, pp. 2732–2739, Jun. 2010.

[17] Y. Wang, W. Yu, C. Wang, and X. Liu, "A modified four-component decomposition method with refined volume scattering models," *IEEE J. Sel. Topics Appl. Earth Observ. Remote Sens.*, vol. 13, pp. 1946–1958, Apr. 2020, doi: 10.1109/JSTARS.2020.2990691.

[18] S. Quan, B. Xiong, D. Xiang, C. Hu, and G. Kuang, "Scattering characterization of obliquely oriented buildings from PolSAR data using eigenvalue-related model," *Remote Sens.*, vol. 11, no. 5, 2019, Art. no. 581.

[19] D. Ratha, D. Mandal, V. Kumar, H. McNairn, A. Bhattacharya, and A. C. Frery, "A generalized volume scattering model-based vegetation index from polarimetric SAR data," *IEEE Geosci. Remote Sens. Lett.*, vol. 16, no. 11, pp. 1791–1795, Nov. 2019.

[20] G. Singh and Y. Yamaguchi, "Model-based six-component scattering matrix power decomposition," *IEEE Trans. Geosci. Remote Sens.*, vol. 56, no. 10, pp. 5687–5704, Oct. 2018.

[21] G. Singh et al., "Seven-component scattering power decomposition of POLSAR coherency matrix," *IEEE Trans. Geosci. Remote Sens.*, vol. 57, no. 11, pp. 8371–8382, Nov. 2019.

[22] D. Xiang, Y. Ban, and Y. Su, "Model-based decomposition with cross scattering for polarimetric SAR urban areas," *IEEE Geosci. Remote Sens. Lett.*, vol. 12, no. 12, pp. 2496–2500, Dec. 2015.

[23] H. Fan, S. Quan, D. Dai, X. Wang, and S. Xiao, "Seven-component model-based decomposition for PolSAR data with sophisticated scattering models," *Remote Sens.*, vol. 11, no. 23, 2019, Art. no. 2802, doi: 10.3390/rs11232802.

[24] R. Malik, G. Singh, O. Dikshit, and Y. Yamaguchi, "General five-component scattering power decomposition with unitary transformation (G5U) of coherency matrix," *Remote Sens.*, vol. 15, 2023, Art. no. 1332.

[25] Y. Wang, W. Yu, and W. Hou, "Five-component decomposition methods of polarimetric SAR and polarimetric SAR interferometry using coupling scattering mechanisms," *IEEE J. Sel. Topics Appl. Earth Observ. Remote Sens.*, vol. 14, pp. 6662–6676, Apr. 2021, doi: 10.1109/JSTARS.2021.3071161.

[26] S. Quan, T. Zhang, W. Wang, G. Kuang, X. Wang, and B. Zeng, "Exploring fine polarimetric decomposition technique for built-up area monitoring," *IEEE Trans. Geosci. Remote Sens.*, vol. 61, Mar. 2023, Art. no. 5204719, doi: 10.1109/TGRS.2023.3257773.

[27] W. An and M. Lin, "Generalized polarimetric entropy: Polarimetric information quantitative analyses of model-based incoherent polarimetric decomposition," *IEEE Trans. Geosci. Remote Sens.*, vol. 59, no. 3, pp. 2041–2057, Mar. 2021.

[28] J. S. Lee, T. L. Ainsworth, J. P. Kelly, and C. Lopez-Martinez, "Evaluation and bias removal of multilook effect on entropy/alpha/anisotropy in polarimetric SAR decomposition," *IEEE Trans. Geosci. Remote Sens.*, vol. 46, no. 10, pp. 3039–3052, Oct. 2008.

[29] T. L. Ainsworth, D. L. Schuler, and J. S. Lee, "Polarimetric SAR characterization of man-made structures in urban areas using normalized circular-pol correlation coefficients," *Remote Sens. Environ.*, vol. 112, no. 6, pp. 2876–2885, 2008.

[30] J. S. Lee and T. L. Ainsworth, "The effect of orientation angle compensation on coherency matrix and polarimetric target decompositions," *IEEE Trans. Geosci. Remote Sens.*, vol. 49, no. 1, pp. 53–64, Jan. 2011.

[31] J. S. Lee, T. L. Ainsworth, and Y. Wang, "Polarization orientation angle and polarimetric SAR scattering characteristics of steep terrain," *IEEE Trans. Geosci. Remote Sens.*, vol. 56, no. 12, pp. 7272–7281, Dec. 2018.

[32] Y. Wang, T. L. Ainsworth, and J. S. Lee, "A comparison study of polarization orientation angle estimation for rough terrain surface," *IEEE J. Sel. Topics Appl. Earth Observ. Remote Sens.*, vol. 15, pp. 5788–5798, Jul. 2022, doi: 10.1109/JSTARS.2022.3190871.

[33] X. Gan, Y. Wang, D. Duan, and T. Yang, "Dot and segment feature analysis and parameter inversion of a curved and graded Bay bridge from UAVSAR imagery," *IEEE J. Sel. Topics Appl. Earth Observ. Remote Sens.*, vol. 12, no. 3, pp. 910–919, Mar. 2019, doi: 10.1109/JSTARS.2019.2895467.

[34] Y. Ling, Y. Wang, and Y. Zhang, "A subaperture SAR-decomposition algorithm to delineate urban targets of large Azimuth angles and vegetation," in *Proc. 13th Eur. Conf. Synthetic Aperture Radar*, 2021, pp. 1–4.

Canbin Hu received the B.S., M.S., and Ph.D. degrees in information and communication engineering from the National University of Defense Technology, Changsha, China, in 2006, 2008, and 2014, respectively.

From 2011 to 2013, he was a visiting Ph.D. student with the IETR Laboratory, University of Rennes 1, Rennes, France. Since 2021, he has been a Lecture with the College of Information Science and Technology, Beijing University of Chemical Technology, Beijing, China. His research interests include synthetic aperture radar (SAR)/polarimetric SAR image processing, and pattern recognition.

Yifei Wang received the B.E. degree in communication engineering in 2021 from Beijing University of Chemical Technology, Beijing, China, where she is currently working toward the M.S. degree in information and communication engineering.

Her research interests include the polarimetric SAR image processing and applications.

Xiaokun Sun received the B.S. degree in communication engineering from the Xidian University, Xi'an, China, in 2001, and the Ph.D. degree in electronic science and technology from the University of National Defense Technology, Changsha, China, in 2008.

She is currently with the College of Information Science and Technology, Beijing University of Chemical Technology, Beijing, China, as an Associate Research Fellow. Her main research interests include synthetic aperture radar (SAR) satellite calibration and quality assessment, and SAR satellite applications.

Sinong Quan received the B.S. degree in mechanical and electronic engineering from the South China University of Technology, Guangzhou, China, in 2013, and the M.S. and Ph.D. degrees in information and communication engineering from the National University of Defense Technology, Changsha, China, in 2015 and 2019, respectively.

He is currently an Associate Professor with the College of Electronic Science and Technology, National University of Defense Technology. His research interests include polarimetric radar information processing, target detection, pattern recognition, and machine learning.

Deliang Xiang (Member, IEEE) received the B.S. degree in remote sensing science and technology from Wuhan University, Wuhan, China, in 2010, the M.S. degree in photogrammetry and remote sensing from the National University of Defense Technology, Changsha, China, in 2012, and the Ph.D. degree in geoinformatics from the KTH Royal Institute of Technology, Stockholm, Sweden, in 2016.

Since 2020, he has been a Full Professor with Interdisciplinary Research Center for Artificial Intelligence, Beijing University of Chemical Technology, Beijing, China. His research interests include urban remote sensing, synthetic aperture radar (SAR)/polarimetric SAR image processing, artificial intelligence, and pattern recognition.

Dr. Xiang is a Reviewer for the *Remote Sensing of Environment*, *ISPRS Journal of Photogrammetry and Remote Sensing*, IEEE JOURNAL OF SELECTED TOPICS IN APPLIED EARTH OBSERVATIONS AND REMOTE SENSING, IEEE GEOSCIENCE AND REMOTE SENSING LETTERS, and several other international journals in the remote sensing field. In 2019, he was the recipient of the Humboldt Research Fellowship.